Electrochemical Evaluation of a New Type of Corrosion Passivation Layer: Artificially Produced Al 2 O 3 Films on Aluminum

ARTICLE *in* LANGMUIR · APRIL 1998

Impact Factor: 4.46 · DOI: 10.1021/la971322s

5 AUTHORS, INCLUDING:

T. D. Burleigh
New Mexico Institute of Mining and Technology
26 PUBLICATIONS **267** CITATIONS

Electrochemical Evaluation of a New Type of Corrosion Passivation Layer: Artificially Produced Al_2O_3 Films on Aluminum

A. Kuznetsova,[†] T. D. Burleigh,[‡] V. Zhukov,[†] J. Blachere,[‡] and J. T. Yates, Jr.*,[†]

Department of Chemistry, Surface Science Center, and Department of Materials Science, University of Pittsburgh, Pittsburgh, Pennsylvania 15260

Received December 2, 1997. In Final Form: January 30, 1998

A recently developed technique for the artificial production of an Al_2O_3 film on ultrahigh-purity polycrystalline Al samples was employed. Electrochemical impedance spectroscopy (EIS), Auger electron spectroscopy (AES), and grazing angle X-ray diffraction (GAXRD) were used to investigate the artificial oxide film. The growth of aluminum oxide in water vapor (5×10^{-7} Torr) enhanced by 100 eV electron bombardment resulted in an artificial oxide film which exhibited a 10−30-fold improvement in electrical resistance in 3.5% NaCl solution compared to oxide films of the same thickness grown at 300 K in the absence of electron bombardment (thermal excitation only). These measurements suggest that the artificial aluminum oxide film may provide superior corrosion passivation qualities compared to thermally grown oxide films. The amorphous nature of the artificial oxide film was confirmed by GAXRD.

I. Introduction

We have recently discovered a new method for the oxidation of aluminum surfaces. The new oxidation method involves the use of electronic excitation of an oxygen-containing molecule at the surface rather than thermal excitation.[1,2] The oxidation process is caused by electron bombardment of water molecules adsorbed on the surface. It has been found that the electronic activation of adsorbed water (or even thin ice layers at 90 K) leads to the production of an oxide film which exhibits the electronic properties of aluminum oxide. Among these characteristic properties are a 2:3 Al^{3+}/O^{2-} stoichiometric ratio, a characteristic Al_2O_3 bulk plasmon loss at 23.7 eV, and Al(2p) and O(1s) core level binding energies characteristic of Al_2O_3 which differ significantly from binding energies observed for Al metal and water.

The electron impact induced excitation of adsorbed water on an aluminum surface to produce Al_2O_3 is highly efficient.[1] A reaction cross-section of 2.5×10^{-16} cm^2 for 100 eV electrons has been measured. The efficient excitation process leading to oxide film formation is not accompanied by significant electron stimulated desorption of H_2O.[1]

It has been found that the electronic excitation process leading to oxide film formation exhibits a threshold electron energy at 6 ± 1 eV.[2] On the basis of this low-energy threshold, this electronic excitation process is likely to involve dissociative electron attachment in which a temporary negative adsorbed H_2O^- ion is produced, with subsequent dissociation to fragments such as H^- and OH. The OH radical then serves as an efficient oxidizing agent. Films of Al_2O_3 on Al(111) have been grown to ~25 Å thickness using adsorbed H_2O at 300 K and 100 eV electron bombardment. The film growth kinetics are *linear* in time at constant electron current density and constant H_2O flux from a background H_2O pressure of 5×10^{-7} Torr. This behavior is sharply in contrast with the $t^{1/2}$ kinetics observed in the normal thermal oxidation process obeying the Cabrera−Mott mechanism. At an Al_2O_3 film thickness of ~25 Å, it has been found that the rate of electron induced oxide film growth suddenly decreases significantly, and the reasons for this behavior are currently unknown.[2]

This paper is concerned with the electrochemical evaluation of artificial Al_2O_3 films produced by the electron impact excitation of adsorbed H_2O molecules on an aluminum surface undergoing film growth. If such artificial Al_2O_3 films are to be useful in the prevention of the corrosion of aluminum surfaces, it is likely that they will exhibit superior electrical resistance under electrochemical corrosion conditions at open circuit potential. We demonstrate here that artificial Al_2O_3 films produced by 100 eV electron impact on adsorbed water exhibit 10−30 times higher average electrical resistance compared to Al_2O_3 films of the same nominal thickness made by water and air oxidation alone. It is postulated that a low-porosity amorphous Al_2O_3 film is produced by this new oxidation method compared to more porous thermally grown Al_2O_3 films.

II. Experimental Section

The samples of pure polycrystalline aluminum (99.999%, Goodfellow; $1.4 \times 1.4 \times 0.15$ cm^3) were mechanically polished with SiC abrasive paper (600 grit) using a Buehler Minimet polisher and then electropolished in a 1% NaOH solution for periods sufficiently long (300 C/cm^2) to remove the thick oxide layer. Then the samples were placed in an ultrahigh-vacuum chamber pumped by a 360 L/s ion pump, a 150 L/s turbo pump, and a titanium sublimation pump. The base pressure measured after a 12 h bakeout was typically 1.5×10^{-10} Torr. Residual gas analysis was carried out with a quadrupole mass spectrometer (UTI Instruments/100C). The Al samples were cleaned to the final stage with Ar^+ bombardment ($E_{Ar^+} = 1$ keV, $P_{Ar} = 5 \times 10^{-5}$ Torr, $I/A \sim 8$ μA/cm^2) for 2 h. The samples were then annealed at 673 K for 5 min. The cleanliness of the Al surface was measured using a CMA Auger electron spectrometer (Perkin-Elmer, Model 11-010) until, following ion bombardment and annealing, only the Al^0(LMM) feature in the Auger spectrum was observed. On the basis of O(KLL)/Al^0(LMM) intensity ratios of almost zero (unmeasurably small O(KLL) intensity), we estimate that less than 0.01 monolayer of oxygen was present on the cleaned surface.

The electron stimulated oxidation of the aluminum samples was performed using a specially designed broad beam electron

[†] Department of Chemistry, Surface Science Center.
[‡] Department of Materials Science.

(1) Ebinger, H. D.; Yates, J. T., Jr. *Phys. Rev. B* **1988**, *57*, 1976.
(2) Ebinger, H. D.; Yates, J. T. Jr. *Surf. Sci.*, accepted.

S0743-7463(97)01322-X CCC: $15.00
Published on Web 04/04/1998

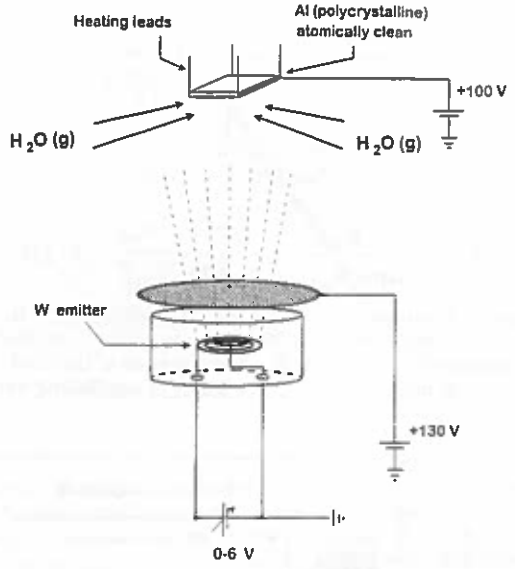

Figure 1. Schematic of the electron gun for electron enhanced oxidation of Al and the geometry of the experiment. The samples are equipped with heating–cooling leads. During electron impact the sample is biased to +100 V relative to ground potential. The extractor grid is biased to +130 V.

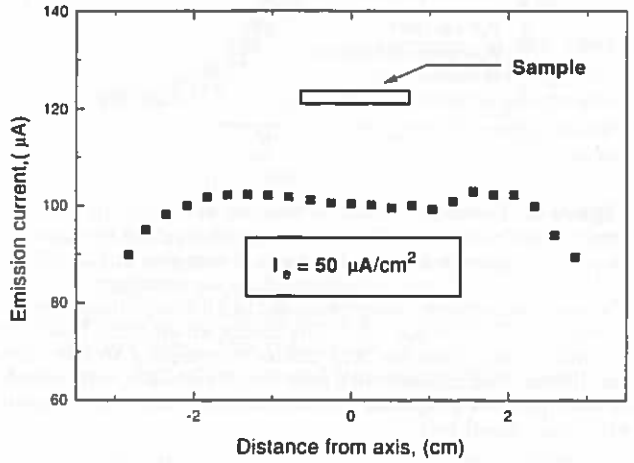

Figure 2. Electron gun emission profile. The sample of 1.96 cm^2 area collected current at a distance of 6 cm along the axis perpendicular to the spiral pancake filament. The current under ultrahigh-vacuum conditions is 50 $\mu A/cm^2$. In the chamber filled with water vapor at $P = 5 \times 10^{-7}$ Torr, the current drops to 30 $\mu A/cm^2$.

gun, shown in Figure 1. A current of 3.5 A ($V = 6$ V) was used to heat the spiral tungsten filament (diameter = 0.25 mm). The accelerator grid was biased to +130 V, which yields the maximum current collected at the Al sample. The emission current density measured at the sample in the chamber was 50 $\mu A/cm^2$, and the average electron energy was 100 eV at the Al sample surface. A uniform emission profile for this electron gun was demonstrated, as shown in Figure 2, with measurements made by a movable collector of 1.96 cm^2 area maintained at +100 V. The current density dropped to 30 $\mu A/cm^2$ when the chamber was filled with water vapor at 5×10^{-7} Torr.

The oxidation was carried out for four samples which were held in the vacuum chamber by a specially designed holder allowing for heating, cooling, and movement of each sample with respect to the electron gun, ion gun, and Auger spectrometer.

The small power input to the Al samples from the electron gun originated from electron bombardment (0.006 W) and radiation from the hot filament (estimated to be 0.02 W). To avoid warming the sample, the support leads were cryogenically cooled and the sample temperature was maintained in the range 298–306 K.

Water vapor from H_2O(l) (deionized and purified by several freeze–pump–thaw cycles) was admitted by means of a leak

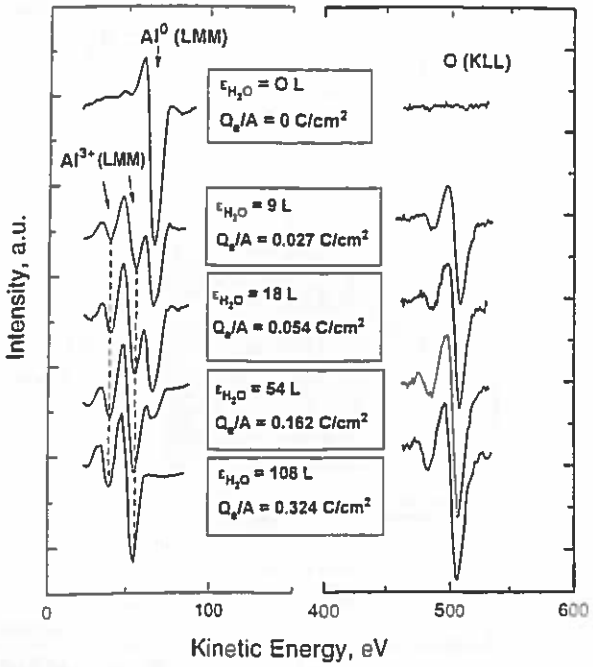

Figure 3. Auger electron spectra of Al^0(LMM), Al^{3+}(LMM), and O(KLL) features in the artificial Al_2O_3/Al film growing in water vapor at $P(H_2O) = 5 \times 10^{-7}$ Torr under the electron beam of 30 $\mu A/cm^2$. The spectra correspond to 0, 9, 18, 54, and 108 langmuirs exposure of water together with 0, 0.027, 0.054, 0.162, and 0.324 C/cm^2 exposure to electrons at 100 eV.

valve to the vacuum chamber at 5×10^{-7} Torr using an uncalibrated Bayard–Alpert gauge for pressure measurement. The mass spectrometer indicated that the water vapor was pure with the major residual gases being H_2, CO, and CO_2, at the 10% level. Under these pressure conditions essentially no gas-phase H_2O molecules are excited by electrons (electron mean free path ~ 20 m). Thus, the electrons activate only adsorbed H_2O molecules in these experiments. Exposure times to electron impact plus water vapor ranged from 2 to 6 h.

Auger spectroscopy studies indicate that extensive electron impact induced oxide film growth occurs under the conditions employed here. Figure 3 shows a sequence of Auger spectra recorded during film growth for various H_2O exposures and electron exposures. In the limit of 3 h of growth, the Auger electron emission from the Al substrate is almost completely suppressed by the oxide overlayer. The oxidation experiments monitored by Auger spectroscopy were performed at $\sim 1 \times 10^{-8}$ Torr pressure followed by pumping to 2×10^{-9} Torr to prevent significant effects of the Auger electron beam on the measurement of the oxide formation by 100 eV electrons. For equivalent electron bombardment times these water exposures were only about 2% of those used to produce the oxide films studied by electrochemical measurements, yet they show the production of very thick oxide films.

To measure the effect of the electron beam on the oxidation behavior and to calibrate the properties of the formed oxide film, control experiments in the absence of electron bombardment were performed in the same chamber. In this case the atomically clean samples were oxidized at 300 K by water vapor at 5×10^{-7} Torr for 2 and 6 h followed by air oxidation at 1 atm during transfer to the electrochemical apparatus.

The electrochemical cell is shown in Figure 4. The conventional three electrode cell includes the reference electrode (saturated calomel, SCE), counter electrode (Pt), and working electrode (WE – Al sample). The electrochemical tests were performed under deaerated conditions provided by a nitrogen gas bubbler; the 99.998% N_2(g) was introduced from a compressed gas cylinder (Liquid Carbonic).

The electrochemical impedance spectroscopy (EIS) tests were done using an EG&G Princeton Applied Research/Model 263 A potentiostat and a Model 5210 lock-in amplifier. The data acquisition was carried out using Model 398 Electrochemical

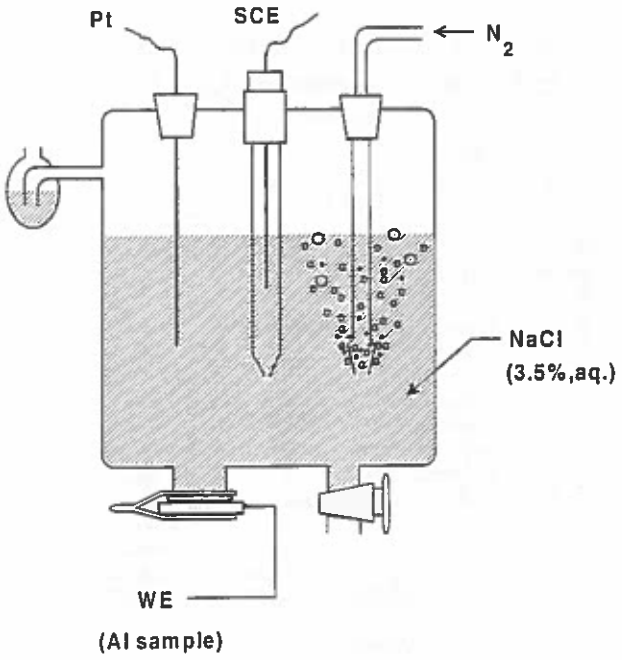

Figure 4. Electrochemical corrosion test cell: aluminum sample working electrode (WE); platinum counter electrode (Pt); saturated calomel electrode (SCE). A nitrogen bubbler eliminates dissolved oxygen.

Impedance Software. All measurements were made at or near the open circuit potential, which was about −0.87 V. The processing of the data and the spectra fitting were done by a nonlinear least-squares method using a commercial graphing program. The impedance spectra were taken in the 10^5 to 0.1 Hz frequency range. The amplitude of the applied potential was at a root mean square value of 5 mV.

A second series of polycrystalline Al samples were prepared using a procedure identical to that employed for the electrochemical measurements. Artificial oxide films, grown by electron bombardment of adsorbed H_2O, and oxide films, grown without electron impact, were studied by grazing angle X-ray diffraction (GAXRD), after transport in air to the diffractometer. A Philips X'pert diffraction instrument was employed using grazing angle X-rays (2° angle of incidence with respect to the grazing angle). A Cu Kα line geometry source was employed with a wavelength $\lambda = 1.5406$ Å.

III. Results

A. Electrochemical Impedance Spectroscopy of Al_2O_3 Films. Electrochemical impedance spectroscopy is a nondestructive technique which uses an electrochemical cell and an applied alternating potential to determine the dependence between the circuit impedance and the frequency.

To minimize the effect of chemistry on the oxide film in the solution, the electrical potential on which the alternating voltage is applied is chosen to be the open circuit potential. This potential corresponds to zero net current in the system. However, as will be shown later, some data suggest that some deterioration of the natural oxide still takes place in saline electrolytes.

The model equivalent circuit describing the impedance characteristics of the electrochemical cell is shown in Figure 5. The oxide film having a resistance, R_{ox}, is in parallel with a capacitor having a film capacitance, C_{ox}. The resistance of the electrolyte is R_{el}. This circuit will exhibit a frequency dependent impedance, Z, as shown by the formula in Figure 5, where f is the ac frequency applied. The impedance is a strong function of f. From the equation it may be seen that at high frequencies the impedance of the circuit is R_{el}, whereas, at very low frequencies, the

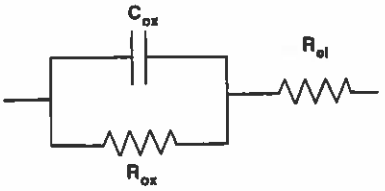

$$Z = R_{el} + \frac{R_{ox}}{1+(2\pi f R_{ox}C_{ox})^2} + \frac{j(-2\pi f R_{ox}^2 C_{ox})}{1+(2\pi f R_{ox}C_{ox})^2}, \quad j=\sqrt{-1}$$

Figure 5. Equivalent circuit used to model (via EIS) the oxide film on aluminum in the 3.5% aqueous solution of NaCl: C_{ox} = capacitance of the oxide; R_{ox} = resistance of the oxide; R_{el} = resistance of electrolyte; f = frequency of oscillating voltage; $j = \sqrt{-1}$.

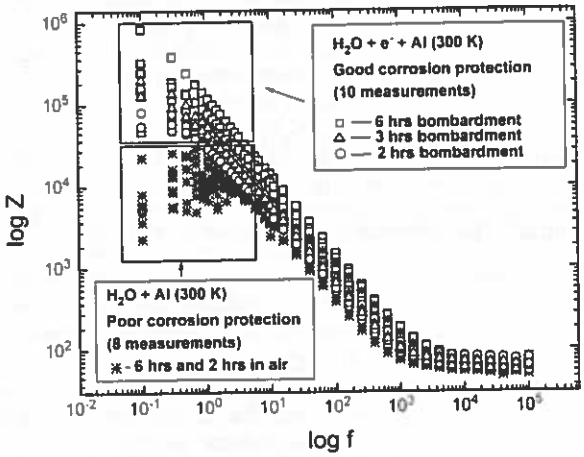

Figure 6. Electrochemical impedance spectroscopy plots for two types of oxidation. The starred symbols show the plots for control samples; water vapor oxidized samples at $P(H_2O) = 5 \times 10^{-7}$ Torr for 2 and 6 h, followed by air exposure at 1 atm. The open square symbols correspond to 6 h of oxidation in water vapor at $P(H_2O) = 5 \times 10^{-7}$ Torr under an electron flux of 30 $\mu A/cm^2$. Open triangles and circles correspond to the same conditions of oxidation with a duration of 3 and 2 h, respectively. All samples were exposed to atmosphere during transfer to the electrochemical cell.

impedance is given by $R_{el} + R_{ox}$. The value of R_{el} in our experiments is about 70 Ω. For frequencies in the range of 10^3 Hz to about 1 Hz the values of R_{el}, R_{ox}, and C_{ox} all contribute to the impedance of the cell. For frequencies below about 1 Hz, the resistance of the oxide film, R_{ox}, is dominant in determining the impedance of the cell.

Figure 6 shows a comparison of the electrochemical impedance spectra for 10 measurements made on 10 samples subjected to H_2O exposure plus electron impact for a period of 2−6 h (open symbols). Following the treatment, these samples were exposed to the atmosphere for 0.5, 1, 1.5, and 2 h before EIS experiments.

Figure 6 also shows the results for 8 control measurements made on 8 Al samples subjected to H_2O exposure without electron impact for a period of 2 or 6 h (starred symbols). Following this treatment, these samples were also exposed to the atmosphere for 0.5, 1, 1.5, and 2 h before EIS measurement. The level of exposure of all samples to the air prior to the electrochemical tests (0.5−2 h) does not correlate with the electrochemical properties measured, suggesting that air exposure following oxidation in the vacuum system is not important in these measurements.

In the frequency region below about 1 Hz, the artificial oxide film grown by electron impact induced dissociation of adsorbed H_2O displays a significantly higher R_{ox} for all

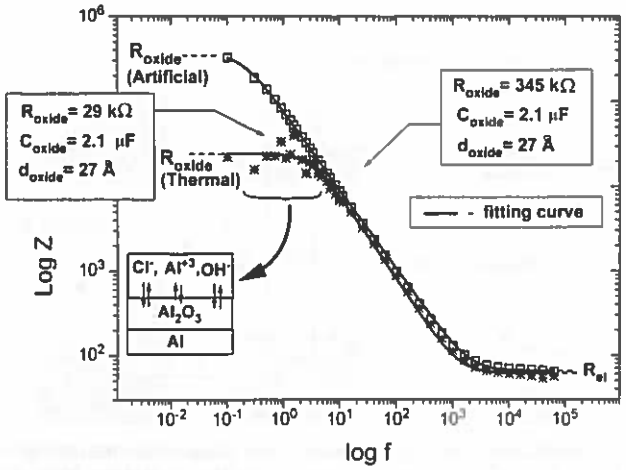

Figure 7. Fitting characteristics of electrochemical impedance plots for two methods of oxide film production. The solid line corresponds to the fitted curve using the equivalent circuit described above in the text. The two oxides were produced over a 6 h exposure. The estimated thickness for both oxides is 27 Å. The factor difference in resistance is 12 for these two samples. The thermally oxidized sample exhibits characteristic scatter of the data near 1 Hz, as do all samples from this series. This is related to the initiation of pitting schematically shown in the figure by ion transport through the oxide film.

10 samples compared to all 8 samples in the control experiment in which electron impact was not employed. The capacitive behavior governing the curve shape as one enters the low-frequency region is typical for all 10 samples oxidized by water vapor combined with electron impact.

The plot shown in Figure 6 allows one to see the statistical spread of the EIS data for 18 aluminum samples. For each EIS experiment, the data were analyzed as shown in Figure 7, where two selected experiments are shown to represent the typical EIS behavior of artificially produced Al_2O_3 compared to the natural oxide. The fitting parameters were the resistance of the oxide film, the resistance of electrolyte, and the capacitance of the oxide using the equivalent circuit shown in Figure 5. The solid line is the fitting curve.

The thickness, d_{ox}, of the oxide was calculated using the conventional formula for a parallel plate capacitor, as given in eq 1, where ϵ = the dielectric constant for

$$d_{ox} = \epsilon\epsilon_0 A/C \qquad (1)$$

aluminum oxide (8.5),[3] ϵ_0 = the permittivity of free space = 8.85×10^{-12} F/m, A = the geometrical area of the sample, and C = the capacitance of the oxide layer. The geometrical surface area exposed to the solution was measured for each sample, and the measured areas agreed to within ±4%.

Figure 7 shows several important features for the electrochemical experiments. Foremost is the 12-fold difference in R_{ox}, comparing the oxide film produced artificially by electron impact and the oxide film grown naturally by exposure to H_2O(g) and to the atmosphere. Both samples were oxidized in the vacuum system for 6 h. We also see that the capacitance of the two films is identical and that the oxide film thickness, based on an assumed dielectric constant of 8.5 for Al_2O_3, is also very similar.

Tables 1 and 2 summarize the 18 measurements comparing the two methods for Al_2O_3 film growth.

Table 1. Characteristics of Al_2O_3 Layer Grown by e^- + H_2O, Followed by Exposure to the Atmosphere

sample	resistance,[a] R_{ox} (kΩ)	capacitance,[a] C_{ox} (μF)	oxide thickness, d_{ox} (Å)
A (6 h)	1130	1.2	47
B (6 h)	58	1.4	40
C (6 h)	345	2.1	27
D (6 h)	234	1.8	31
av	441 ± 343	1.6 ± 0.3	36 ± 7
E (3 h)	212	2.8	20
F (3 h)	118	3.0	17
av	165 ± 47	2.9 ± 0.1	19 ± 2
G (2 h)	141	4.5	13
H (2 h)	158	2.9	21
I (2 h)	52	3.5	17
J (2 h)	73	4.4	14
av	106 ± 44	3.8 ± 0.6	16 ± 3

[a] Numbers obtained from fits to EIS plots.

Table 2. Characteristics of Al_2O_3 Layer Grown by Exposure to H_2O, Followed by Exposure to the Atmosphere

sample	resistance,[a] R_{ox} (kΩ)	capacitance,[a] C_{ox} (μF)	oxide thickness, d_{ox} (Å)
K (6 h)	29	2.1	27
L (6 h)	10	1.6	37
M (6 h)	14	4.1	14
N (6 h)	9	1.2	47
av	16 ± 7	2.3 ± 1.3	31 ± 11
O (2 h)	13	4.4	13
P (2 h)	7	1.8	31
Q (2 h)	13	2.4	24
R (2 h)	9	2.0	28
av	10 ± 3	2.7 ± 0.9	24 ± 6

[a] Numbers obtained from fits to EIS plots.

In Table 1, several trends are evident:

1. An enhanced oxide resistance is developed for increasing e^- + H_2O(g) exposure to a clean aluminum surface.
2. An increase in oxide thickness occurs for increasing e^- + H_2O(g) exposure.
3. The behavior of the oxide layer approaches the ideal capacitive behavior with the increase in exposure to water vapor and exposure to electrons. (The ideal capacitor exhibits inversely proportional dependence between the impedance and frequency, according to the formula $Z = 1/(2\pi jfC)$, where $j = \sqrt{-1}$, f = frequency, and C = capacitance).

Comparing Table 1 to Table 2, one may see that for equivalent H_2O and subsequent atmospheric exposure times, the average value of R_{ox} for the artificially produced Al_2O_3 films exceeds that of the control experiment by a factor ranging from ~30 (6 h exposure) to ~10 (2 h exposure).

The resistivity, ρ, of the Al_2O_3 films may be calculated from the resistance and the oxide thickness, d_{ox}, and the film geometrical area, A, using eq 2.

$$\rho = R_{ox}A/d_{ox} \qquad (2)$$

Table 3 gives the calculated resistivity for each of the 18 samples. The artificial oxide gives a value of resistivity which is the typical value of an insulator, about 10^{11} Ω cm.[4-6] The natural oxide exhibits a resistivity which is more than 1 order of magnitude smaller.

(3) Wernick, S.; Pinner, R.; Sheasby, P. G. *The Surface Treatment and Finishing of Aluminum and Its Alloys*, 5th ed.; ASM International: Metals Park, OH, 1987; Vol. 2.

(4) Lide, D. R. *Handbook of Chemistry and Physics*; CRC Press: Boca Raton, FL, 1993–1994.

Table 3. Comparison of Resistivities of Al_2O_3 Layers

sample	resistivity, ρ (Ω cm)
Artificial Oxide Film	
A (6 h)	1.8×10^{12}
B (6 h)	1.1×10^{11}
C (6 h)	1.2×10^{12}
D (6 h)	5.7×10^{11}
av	$(9.2 \pm 5.8) \times 10^{11}$
E (3 h)	7.8×10^{11}
F (3 h)	4.6×10^{11}
av	$(6.2 \pm 1.6) \times 10^{11}$
G (2 h)	8.3×10^{11}
H (2 h)	6.0×10^{11}
I (2 h)	2.4×10^{11}
J (2 h)	4.2×10^{11}
av	$(5.2 \pm 1.9) \times 10^{11}$
Control Oxide Film	
K (6 h)	8.0×10^{10}
L (6 h)	2.1×10^{10}
M (6 h)	7.6×10^{10}
N (6 h)	1.4×10^{10}
av	$(4.8 \pm 3.0) \times 10^{10}$
O (2 h)	7.6×10^{10}
P (2 h)	1.6×10^{10}
Q (2 h)	4.1×10^{10}
R. (2 h)	2.3×10^{10}
av	$(3.9 \pm 1.9) \times 10^{10}$

B. Electrochemical Noise at Low Frequency in EIS Measurements. The values of the impedance of the oxide film and with the scatter factor due to fluctuations in the impedance (chemical noise) are both indicators of the film resistance to electrochemical corrosion.[7] Figure 8 shows a comparison of the electrochemical noise for the two types of Al_2O_3 films. On the basis of these two electrochemical measurement criteria, the artificial oxide films are superior to the thermally grown oxide films since the artificial films exhibit high impedance and low electrochemical noise. It is known that in Cl^-(aq) solution pitting corrosion will be induced as breakdown of the oxide film occurs, and this is a major attack mechanism in the corrosion of aluminum and aluminum alloy surfaces.[8]

C. Grazing Angle X-ray Diffraction Studies. Four Al_2O_3 films were investigated by GAXRD. These oxide films were supported on polycrystalline Al substrates, produced by artificial and natural oxidation methods identical to those used for the electrochemical experiments. These were compared using grazing angle X-ray diffraction in an attempt to determine whether a crystalline oxide phase exists in either case. The results of this analysis are shown in Figure 9. The GAXRD spectra differ in the intensity of diffraction features due to the differing Al crystallite orientation present in the polycrystalline samples. Diffraction features from the Al crystallites underlaying the Al_2O_3 film dominate.

Two additional low-intensity GAXRD features may be recognized in both the H_2O + air-oxidized and in the e^- + H_2O + air-oxidized samples. These features, shown by index marks, correspond to interatomic spacings of 2.232 ± 0.003 and 2.108 ± 0.002 Å and may be due to small quantities of crystalline material in the oxide films. It is noted, however, that these two features are present in both the artificially produced Al_2O_3 film and in the natural oxide film.

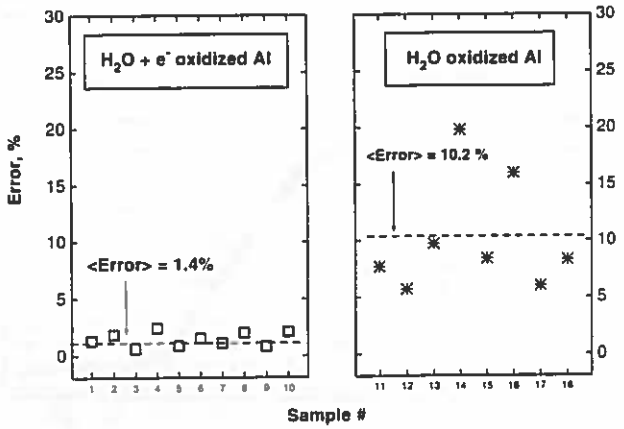

Figure 8. Scatter in the data points in the low-frequency region (f < 1 Hz) of EIS plots, presented as the deviation from the mean of the measurements of R_{ox} estimated by the fitting technique for 18 samples. Each data point corresponds to one sample. The average deviation is 1.4% for the artificial oxide and 10.2% for the natural oxide.

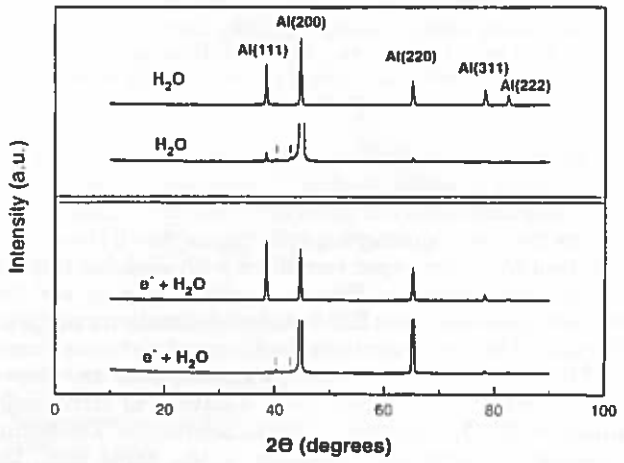

Figure 9. Grazing angle X-ray diffraction patterns for the two oxides. The X-rays were directed at 2° incidence angle with respect to grazing. A line source with a 0.0825° slit was used. The scans were taken from 10 to 90°. Two XRD patterns correspond to two different samples oxidized in H_2O. Two samples oxidized by e^- + H_2O are also shown. The samples were exposed to atmosphere for about 24 h after they were taken from the ultrahigh-vacuum chamber.

These GAXRD results show that the electrochemical differences observed between the artificial oxide and the natural oxide films are not related to issues of Al_2O_3 crystallinity and that the differences must lie in variations in the nature of the amorphous Al_2O_3 layer.

IV. Discussion

A. Electron Impact Induced Oxidation of Al. The mechanism of the electronic excitation of adsorbed water molecules was discussed in previous papers.[1-2] Dissociative electron attachment of adsorbed H_2O produces highly reactive species. These surface species could be OH^-, the OH radical, or hot oxygen atoms.[9] Oxidation, induced by the nonequilibrium production of active oxygen-bearing species, dominates in the production of the artificial oxide film.

The artificial oxidation mechanism contrasts with the natural oxide growth in the atmosphere or in water vapor. The principal difference between the first step of the

(5) Wefers, K.; Misra, C. *Oxides and Hydroxides of Aluminum*; Alcoa Laboratories: Pittsburgh, PA, 1987.
(6) Diggle, J. *Oxides and Oxide Films*; Dekker: New York, 1972.
(7) Mansfeld, F. *Second International Symposium on Electrochemical Impedance Spectroscopy*, July 12–17, 1992, Santa Barbara, CA.
(8) Szklarska-Smialowska, Z. In *Pitting Corrosion of Metals*; NACE: Houston, TX, 1986.
(9) Curtis, M. G.; Walker, I. C. *J. Chem. Soc., Faraday Trans.* **1992**, *88*, 2805.

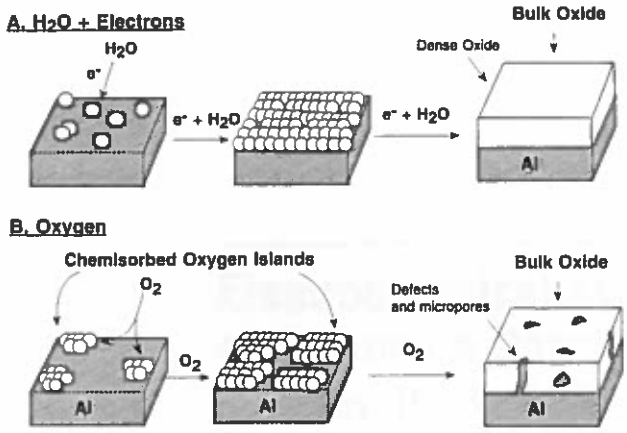

Figure 10. Schematic of oxidation of aluminum at 300 K (A) by H_2O + electrons; (B) by oxygen.

electron induced process and the thermally activated oxidation in oxygen is the formation of oxide islands as precursors for bulk oxide formation in the thermal process. At small oxygen coverages, this process can be schematically depicted by the first step of oxidation shown in Figure 10B. The oxygen atoms chemisorbed on the aluminum surface form islands as a result of attractive forces at island edges. With higher exposures the surface becomes covered completely with oxide islands of 20 Å size.[10,11] The oxidation mechanism producing a thicker Al_2O_3 film is a more complicated process controlled by the gradients in chemical and electrical potentials. The mechanism of the thermally activated production of thin oxide films on pure aluminum is explained by the Cabrera–Mott theory, which was developed in 1949[12] and still is the most reliable theory for the growth of thin oxide films. According to this mechanism, the limiting kinetic step in oxidation is ion diffusion. The electrons from the metal can pass through an oxide layer of 100 Å thickness or less. The oxygen-containing species trap these electrons, causing conversion into oxygen anions. The estimated potential drop across the oxide film is of the order of 1 V; for a 30 Å film an electric field of about 3×10^6 V/cm exists which is high enough to drive ions through the growing oxide film.

The production of localized island structures of Al_2O_3 on Al may lead to a relatively porous film structure as schematically shown at the end of the sequence in Figure 10B.

In contrast to the thermally activated oxidation process, electronic activation of reactive oxidizing species leads to very efficient oxide film formation even at 90 K.[1] The kinetic details of this process are not understood, but it is possible that the cluster formation and island growth of Al_2O_3 (both characteristic of thermal oxidation) do not occur when electron induced oxidation processes are at work during the initial steps of oxidation, as schematically indicated in Figure 10A. Moreover, the linear growth kinetics for the artificial oxide film formation, driven by a *constant* electric field through the growing oxide film,[2] differs from the $t^{1/2}$ kinetics of the Cabrera–Mott mechanism and may lead to a different film growth morphology which does not end with a microporous oxide film. Such a nonporous oxide film is indicated at the end of the sequence shown in Figure 10A.

(10) Brune, H.; Wintterlin, J.; Trost, J.; Ertl, G. *J. Chem. Phys.* **1993**, *99*, 2128.
(11) Trost, J.; Brune, H.; Wintterlin, J.; Behm, R. J.; Ertl, G. *J. Chem. Phys.* **1988**, *108*, 1740.
(12) Cabrera, N.; Mott, N. F. *Rep. Prog. Phys.* **1949**, *12*, 163.

B. Corrosion Passivation by Artificial Oxide Film. The electrical resistance of the oxide film on an aluminum surface should be an excellent indicator of its corrosion inhibition behavior. This is because metal corrosion involves ion transport, often from electrolyte solutions in contact with the oxide surface.

Two prominent differences in electrochemical characteristics are noted in the electrochemical impedance spectroscopy measurements, comparing thermally oxidized aluminum and artificially oxidized aluminum surfaces:

1. The average electrical resistances of the artificial oxide films compared to the thermally oxidized films of equivalent thickness are 10–30 times higher, as may be seen in Figures 6 and 7.

2. The scatter in the EIS data near 1 Hz frequency for individual measurements on the thermally oxidized aluminum surface is significantly higher than for the artificial oxide surface, as may be seen in Figure 8. This may indicate the improved resistance of the artificial film to chemical breakdown under electrochemical conditions.

C. Morphology of Al_2O_3 Films. The thermal oxidation of aluminum in air ($T < 450$ °C) is known to produce an amorphous Al_2O_3 film of limited thickness (30–40 Å).[13] This has been seen in our studies of the 300 K oxidized surface using grazing angle X-ray diffraction. Electron impact induced oxidation also produces amorphous aluminum oxide films, indicating that the increased electrical resistance of these films cannot be attributed to the production of crystalline Al_2O_3.

V. Summary of Results

A new method for the artificial production of Al_2O_3 films on pure aluminum surfaces has been studied using Auger electron spectroscopy, electrochemical impedance spectroscopy, and grazing angle X-ray diffraction. The new oxidation method involves the electronic activation of adsorbed water molecules to initiate surface oxidation. Very efficient oxidation is achieved by 100 eV electron impact on aluminum surfaces exposed to $H_2O(g)$ at 5×10^{-7} Torr and at 300 K.

Electrochemical impedance measurements on the electron bombarded surfaces indicate a 10–30-fold increase in oxide film electrical resistance compared to films of similar thickness and capacitance made with identical exposure to H_2O. Both oxidation treatments are followed by exposure to air at atmospheric pressure, which is not believed to affect the film characteristics in either case. In addition, the electron bombarded surfaces show less fluctuation in impedance below 1 Hz compared to the 300 K oxidized films, suggesting superior corrosion resistance for the artificial oxide film.

The differences in the electrochemical properties are attributed to the reduction of film porosity for the artificial oxide films compared to naturally grown oxide films, leading to greater resistance to electrochemical corrosion in NaCl(aq) media.

Acknowledgment. The full support of the Air Force Office of Scientific Research is gratefully acknowledged.

LA971322S

(13) Godard, H. *The Corrosion of Light Metals;* Wiley: New York, London, Sydney, 1967; and references cited therein.

Electrochemical Evaluation of a New Type of Corrosion Passivation Layer: Artificially Produced Al_2O_3 Films on Aluminum

A. Kuznetsova, T. D. Burleigh, V. Zhukov, J. Blachere, and J. T. Yates, Jr.

Department of Chemistry, Surface Science Center, and Department of Materials Science, University of Pittsburgh, Pittsburgh, Pennsylvania 15260

Langmuir®
The ACS Journal of Surfaces and Colloids

Reprinted from
Volume 14, Number 9, Pages 2502–2507